Runaway electrons in a tokamak: A free-electron maser

B. Kurzan and K.-H. Steuer
Max-Planck-Institut für Plasmaphysik, Euratom-IPP Association, D-85748 Garching, Germany
(Received 26 September 1995; revised manuscript received 23 December 1996)

In ohmic divertor plasma discharges of the ASDEX upgrade tokamak containing a small population of runaway electrons, fluctuating emission in the microwave region with a very narrow bandwidth is observed. The radiation can be explained by relativistic runaway electrons, which are captured in a ripple resonance of the tokamak and are thus made monoenergetic enough that they can undergo the collective instability of a free-electron maser. From the frequency of the maser, the energy of the runaway electrons, and from the linewidth and energy per radiation pulse, the particle density of the runaway electrons is determined locally. Observing this maser radiation is thus a different diagnostic for runaway electrons in tokamaks. [S1063-651X(97)12104-3]

PACS number(s): 52.25.Sw, 52.75.Ms

INTRODUCTION

For electrons moving faster than the mean thermal velocity, the friction force due to collisions decreases with increasing velocity. Thus with an electric field present in the plasma such electrons are continuously accelerated, resulting in runaway particles [1]. The dynamics of runaway electrons in tokamaks can be described by a Fokker-Planck equation [2], taking into account the acceleration in the toroidal electric field, the deceleration by synchrotron radiation losses, the effect of collisions, and the ripple resonance mechanism. With the last mechanism the angle between the velocity of the runaway electrons and the magnetic field, the so-called pitch angle, is increased, if the runaway electrons' gyromotion is resonant with the harmonics of the magnetic ripple of the tokamak. If the increased synchrotron losses of the runaway electrons equal the energy gain in the toroidal electric field, the energy of the runaway electrons stays constant. This is clearly seen in the bremsstrahlung spectra of the runaway electrons obtained on the axial symmetric divertor experiment (ASDEX) [2]. These relativistic monoenergetic runaway electrons amplify their spontaneously emitted radiation in the microwave range as a free-electron maser, which is the subject of this article. The maser radiation is clearly seen in the ASDEX upgrade tokamak [3] as fluctuating emission.

DETECTION SYSTEM

The apparatus [4] used for the detection of the radiation is a polychromator system usually used for the measurement of the temperature of the thermal electrons. The system detects microwaves, which are emitted and polarized perpendicularly to the magnetic field. It consists of several channels, which are sensitive to different microwave frequencies. Each channel covers a spectral range of 2.6 GHz. Due to technical restrictions, the detection frequencies cannot be adjusted independently for each channel, but only for groups of four channels. The channels of one group have a fixed difference of about 4 GHz between their sensitive spectral ranges. The detectors are InSb hot electron bolometers. The time resolution (integrating time constant) of the system, consisting of the detectors and the amplifiers is 1 ms.

OBSERVATION

By delaying the density ramp up at the beginning of an ohmic plasma discharge, a small runaway electron population is purposely generated. The current carried by the runaway electrons never exceeds 10 kA, which is concluded from evaluating the absolutely calibrated hard-x-ray intensity generated by the runaway electrons. In an ohmic single-null divertor discharge (nominal magnetic field 2.90 T, plasma current 600 kA, line-averaged thermal electron density 3×10^{19} m^{-3}) containing runaway electrons generated at the time $t=0.35\pm0.01$ s by the above method fluctuating emission (spikes) with frequency 116 ± 2 GHz starts to develop at the time 1.8 s (Fig. 1). Spikes at other frequencies of the microwave region develop in discharges with other values of the plasma density and the magnetic field (see below). This phenomenon has not yet been explained.

INTERPRETATION OF THE SPIKES AS MASER RADIATION

The power of the fluctuating emission is much bigger than the continuously emitted spontaneous radiation, which in Fig. 1 is practically zero. There is also no radiation from the plasma (plasma frequencies, cyclotron radiation) that can account for the spikes. So the narrow emission must be radiation amplified by the runaway electrons. The Parail-Pogutse instability of suprathermal electrons [5] could amplify radiation via the anormal Doppler effect. Since no suprathermal electrons are generated during the time of the fluctuating emission and the anormal Doppler effect is not possible for the refractive index of the plasma, which is smaller or equal to one (Fig. 5), this instability must be excluded.

Solving the time-dependent Fokker-Planck equation describing the dynamics of runaway electrons in tokamaks [2] for the discharge discussed (where the skin effect is also taken into account [6]) gives different final energies of the runaway electrons, depending on the position of their drift surfaces in the plasma: Near the plasma center (minor radius

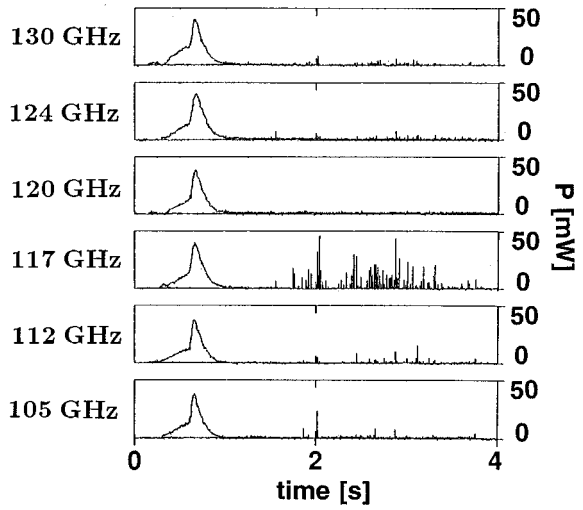

FIG. 1. Total radiated power P of the runaway electrons emitted in a direction perpendicular to the path of the runaway electrons in the microwave region, which is scaled from the radiation detected by the polychromator system [4] with an integration time constant of 1 ms: the continuous emission in the first second of the discharge stems from the just generated suprathermal electrons. With increasing energy of the runaway electrons this emission is shifted to higher frequencies. When the runaway electrons have reached their maximum energy, fluctuating emission (spikes) starts to develop in the channel, which is sensitive to radiation with frequency 117 GHz. Since in the neighboring channels the intensity of the spikes is much lower, the emission frequency is 116 ± 2 GHz.

$r\approx0$) the runaway electrons are accelerated to very high energies, since due to the small ripple there is no effective energy barrier. Near the plasma edge ($r\approx a$) the runaway electrons are captured at very low energies in a ripple resonance, because of the strong ripple there. Since with [7] one can assume for the runaway electrons the same near-parabolic density profile as measured for the thermal electrons, the energy which is finally reached at these two positions applies only to a minority of the population. In a region around $r=a/\sqrt{3}$ where the majority of the runaway population is located, the runaway electrons are captured in the toroidal $n=8$ resonance (strength of the ripple relative to the toroidal magnetic field $\Delta B/B=8\times10^{-7}$) corresponding to an energy of 11.5 MeV, which is characteristic of the majority of runaway electrons. The just mentioned small relative ripple induces no additional spontaneous emission, which could explain the fluctuating emission.

The time-independent Fokker-Planck equation near the $n=8$ resonance was solved numerically with the simplification, that the ripple resonance is effective at a constant resonant momentum $p_r=p_{nm}(\vartheta=0$ rad) (p_{nm} is the momentum resonant with the nth toroidal and mth poloidal ripple harmonic [2], ϑ is the pitch angle of the runaway electrons) and not at constant gyrocenter momentum $p_{nm}(\vartheta)=p_r/\cos(\vartheta)$ [8]. According to this solution (Fig. 2) the runaway electrons have a very narrow energy distribution $\Delta p/p_r\approx8\times10^{-3}$ at $p_r=22.5m_ec$ (m_e is the electron rest mass and c is the speed of light in vacuum) and a maximum at the pitch angle $\vartheta_M=0.207$ rad corresponding to $\cos(\vartheta_M)=0.9786$. Due to the simplification made, the correct resonant momentum is $p_{nm}(\vartheta_M)=p_r/\cos(\vartheta_M)=23.0m_ec$. The runaway electrons

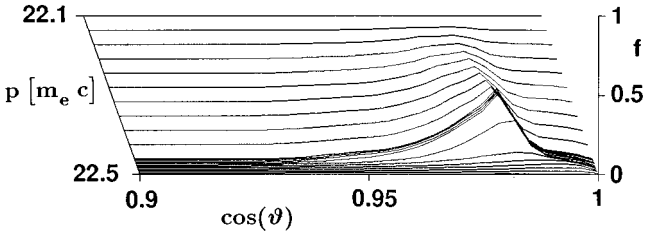

FIG. 2. Calculated stationary distribution of the runaway electrons captured in the $n=8$ resonance.

have both a narrow gyrocenter momentum and gyromomentum distribution. The extent of the calculated momentum distribution in the direction of the pitch angle is, however, broader than the real one, because the resonant isotropization of the pitch angle is more effective with the constant resonance momentum assumed here for the calculation, than with the real resonant momentum, which depends on the pitch angle.

This extremely monoenergetic runaway electron beam can amplify radiation as a free-electron maser, as will be shown. Since in a tokamak the helical motion of the electron beam stems from the gyromotion of the runaway electrons in the confining magnetic field, the energy blocked runaway electrons form a so-called cyclotron-auto-resonance-maser (CARM) originally proposed by [9,10]. The instability can be triggered by an electromagnetic wave moving parallel to the gyrocenter velocity [6] of the runaway electrons and possessing the resonant frequency

$$\nu=\frac{\nu_{ce}}{1-n\beta_r\cos(\vartheta_M)} \tag{1}$$

[n is the refractive index, $\beta_r=\sqrt{1-1/\gamma_r^2}$, γ_r is the relativistic γ factor of the runaway electrons, $\nu_{ce}=(eB)/(2\pi\gamma_r m_e)$ is the gyrofrequency of the runaway electrons, e is the elementary charge, and B is the toroidal magnetic field].

The initial resonant electromagnetic wave is emitted spontaneously by the runaway electrons via the normal Doppler effect everywhere in the plasma volume. Since $B\sim1/R$ and so $\nu_{ce}\sim1/R$, where R is the major radius of the plasma varying between 1.05 m and 2.15 m, one should expect a much broader emission spectrum than observed. The CARM process, however, is only possible at certain major radii by which the observed frequency is defined: The initial wave, which is emitted by the relativistic electrons into a cone of width $1/\gamma_r$ rad in the direction of their momentary velocity, does not immediately run parallel to the gyrocenter velocity of the runaway electrons, but encloses with this direction the angle α, which is initially equal to the pitch angle $\vartheta_M\gg1/\gamma_r$ rad. So the electromagnetic wave cannot interact with the electron beam *a priori*. This electromagnetic wave with frequency $\nu=\nu_{ce}/[1-n(\alpha)\cos(\alpha)\beta_r\cos(\vartheta_M)]$ interacts with the medium consisting of the plasma and the runaways for which the refractive index was calculated (Appendix A). At the position where the frequency of the spontaneously emitted radiation is resonant with the Doppler shifted gyrofrequency of the runaways, the refractive index of the medium depends only weakly on the runaway density, but is mainly determined by the runaway electrons' resonance de-

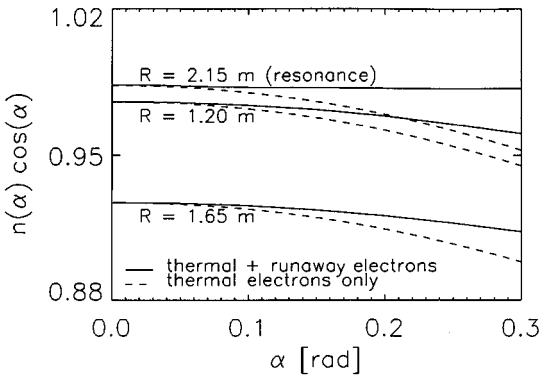

FIG. 3. For a plasma runaway electron medium (Appendix A) $n(\alpha)\cos(\alpha)$ is nearly constant if the frequency of the propagating wave is in resonance with the Doppler shifted gyrofrequency of the runaways, which is the case at the major radius 2.15 m. This is impossible for the pure plasma. At other major radii the runaways change the refractive index compared to the pure plasma case, but $n(\alpha)\cos(\alpha)$ is not constant. The results shown here are calculated with a parabolic profile for the thermal electron density for $|R-1.65\text{m}|<0.5$ m and an exponentially decaying profile (decay constant ≈ 1 cm) for $|R-1.65\ \text{m}|>0.5$ m as observed on ASDEX upgrade.

nominator $D_R=2\pi\gamma_r\{\nu[1-n(\alpha)\cos(\alpha)\cos(\vartheta_M)\beta_r]-\nu_{ce}\}\approx 0$. At the resonance the product term $n(\alpha)\cos(\alpha)$ is nearly constant when varying α, because D_R stays near to zero (Fig. 3). Thus the frequency of the radiation emitted with angle $\alpha\neq 0$ at the resonance position is approximately the same as for $\alpha=0$. Another consequence is that the radiation initially emitted with $\alpha=\vartheta_M$ is bent to $\alpha=0$ so that it finally runs parallel with the guiding center velocity of the runaways (Fig. 4). This wave, however, is shifted in the poloidal plane of the tokamak by about 1 cm with respect to the position of the emission. The displaced wave can only interact resonantly with the runaway electrons if the resonance frequency ν does not change with the position,

$$\vec{\nabla}\nu=\vec{0}. \tag{2}$$

This condition is fulfilled if the refractive index for the wave

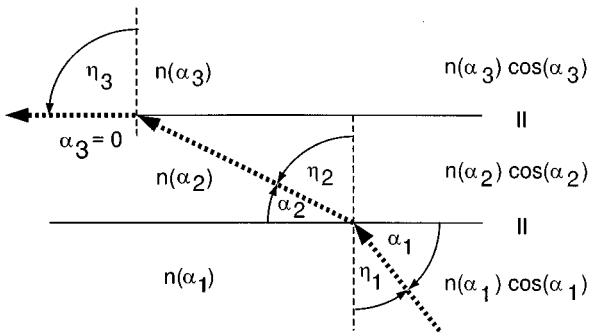

FIG. 4. An electromagnetic wave, propagating initially with angle $\alpha\neq 0$ with respect to the magnetic field, is bent to $\alpha=0$ if, according to the laws of refraction, $n(\eta)\sin(\eta)=n(\alpha)\cos(\alpha)=\text{const}$ is fulfilled, as is the case for the plasma runaway electron medium.

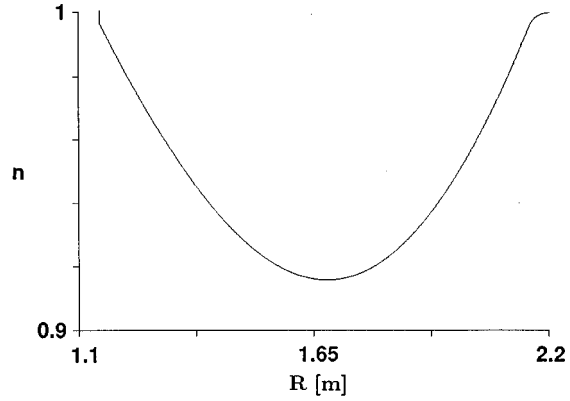

FIG. 5. Refractive index for an electromagnetic wave of frequency 116 GHz propagating parallel to the magnetic field in the equatorial plane of a cold plasma, calculated with the density profile used in Fig. 3.

propagating parallel to the magnetic field varies in the poloidal (R,z) plane of the tokamak as

$$\left(\frac{dn}{dz}\right)_{\text{post}}=0$$

$$\left(\frac{dn}{dR}\right)_{\text{post}}=\left[\frac{1}{\beta_r\cos(\vartheta_M)}-n(\alpha=0,R)\right]\Big/ R. \tag{3}$$

For propagation with $\alpha=0$, the refractive index is mainly determined by the plasma alone (Fig. 3). The refractive index for a cold plasma [11] depends on both the density of the thermal electrons and the magnetic field (Fig. 5). The latter, however, does not change with z. So $(dn/dz)_{\text{post}}=0$ is only fulfilled in the equatorial plane of the plasma, where the flux surfaces on which the electron density is constant are tangential to the z direction. Comparing the postulated change $(dn/dR)_{\text{post}}$ with the real change (dn/dR) in the equatorial plane of the plasma gives two major radii where both match and the CARM process is possible (Fig. 6). However, it is only at the plasma edge ($R=2.15$ m) that the calculated frequency 122 ± 9 GHz agrees with the observed frequency

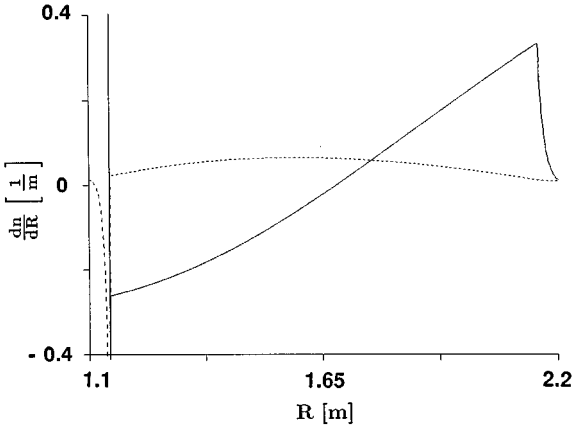

FIG. 6. Comparison between the real (dn/dR) (solid line) and the postulated $(dn/dR)_{\text{post}}$ (dotted line) in the equatorial plane of the plasma.

116 ± 2 GHz. The resonant position at the plasma edge exists only for an exponentially decaying thermal electron density as observed in the scrape-off layer of ASDEX upgrade.

COHERENCE LENGTH

The width $2\Delta\nu_{1/2} \lesssim 4$ GHz of the amplified spontaneous emission must be due to a monochromatic wave pulse of length [12]

$$L_P \gtrsim \frac{\nu}{2\Delta\nu_{1/2}} \frac{v_{GC}}{\nu_{ce}} = 3.2 \text{ m} \tag{4}$$

(v_{GC} is the guiding center velocity [6] of the runaways). This wave pulse is long enough, that for the time of the interaction it is bent along the runaway paths with a radius of curvature of about $R_C = 2.15$ m. This is possible in the plasma runaway electron medium, as shown above (Figs. 3 and 4). Thus, in addition to an amplifying fiber, a halo of runaway electrons with a diameter of some centimeters around the core is necessary to make the maser process possible in the tokamak. This condition is fulfilled since, over a length of some centimeters, the runaways are uniformly distributed in the plasma. The value of L_P obtained here is consistent with the observed efficiency of the maser calculated below.

DETERMINATION OF THE RUNAWAY ELECTRON DENSITY, GAIN OF THE CARM

The finite length L_P is due to the loss L of the curved guided wave,

$$L = \exp\left(-\frac{v_{GC} t}{L_P}\right). \tag{5}$$

For the emission of coherent radiation this must be compensated by the gain G of the CARM. G increases with the density n_R of the runaway electrons. For an overall amplification greater than one, the condition $G \times L \gtrsim 1$ must be fulfilled, thus giving a lower limit for the density of the runaways. For this, the gain of the CARM, parametrized by n_R, must be calculated.

The potentially amplifying electron beam is embedded in the edge plasma of ASDEX upgrade (thermal electron density $n_e = 10^{18}$ m^{-3}, magnetic field $B = 2.23$ T), which could affect the gain of the CARM. This is discussed in the following.

The observed radiation could be shielded by the plasma if the plasma frequency ν_{pe0} is bigger than the frequency of the CARM. The plasma density, however, is so small that the resulting plasma frequency $\nu_{pe0} = 9$ GHz is much smaller than the frequency 116 GHz of the CARM. Thus the effect of the shielding can be neglected.

The bunching of the runaway electrons during the masing process (Appendix B) is not perturbed by collisions of the runaway electrons with the plasma particles, because their mean free path length $l = 1/(\sigma n_e)$ (σ is an effective cross section) is much greater than the interaction length L_P. The effective cross section describing the collisions of the runaway electrons with the thermal ions and electrons is calculated by

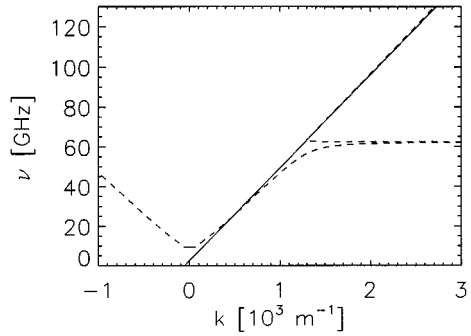

FIG. 7. Brillouin plot of the dispersive characteristics of the CARM, $\nu = k\cos(\vartheta_M) v_{GC} + \nu_{ce}$ (solid line) and of the tokamak edge plasma ($n_e = 10^{18}$ m^{-3}, $B = 2.23$ T) (dashed line) possessing a cyclotron resonance at 62 GHz (shot no. 4770) (ν is the frequency and k is the wave number). No electromagnetic wave can propagate below the plasma frequency $\nu_{pe0} = 9$ GHz at $k = 0$. The dispersion relations of the beam and the plasma intersect only for positive wave numbers, thus no counterrunning wave is possible.

$$\sigma = \int_{\theta_{\min}}^{\theta_{\max}} \frac{d\sigma}{d\theta} \theta^2 d\theta \tag{6}$$

($d\sigma/d\theta$ is the differential cross section, θ is the angle between the velocity vectors of the runaway electron before and after a collision). Using the relativistically correct differential cross section [13], the mean free path length of the relativistic runaway electrons moving at the speed of light is

$$l = \frac{e \pi \varepsilon_0^2 m_e^2 c^4 \gamma_r^2}{e^4 (Z_{\text{eff}} + 1) \ln(\Lambda) n_e} \tag{7}$$

[ε_0 is the dielectric constant, Z_{eff} is the effective ion charge of the plasma, $\ln(\Lambda) = \ln(\theta_{\max}/\theta_{\min}) = 17$ is the Coulomb logarithm]. For the runaway electrons of interest here, $\gamma_r = 23$, the thermal electron density $n_e = 10^{18}$ m^{-3}, and a pure hydrogen plasma ($Z_{\text{eff}} = 1$) the mean free path length $l = 7.8 \times 10^{10}$ m is much bigger than L_P. Thus the runaway electrons are collisionless along the interaction length L_P.

For the CARM formed by the runaway electrons no counterrunning wave [14], but only corunning waves are possible for the above mentioned parameters of the plasma (see Fig. 7). Thus when calculating the gain of the CARM the following effects arising from the presence of a counterrunning wave can be neglected: There is no energy exchange between the co-, and counterrunning wave and the electron beam [15], no induction of a Bragg reflecting density grating in the plasma surrounding the beam [16], no coherent addition of co- and counterrunning wave [17]. These effects could influence the coupling between the electromagnetic waves and the electron beam and thus the CARM's gain. The small change of the refractive index at the observed frequency of 116 GHz between the cases of pure vacuum and plasma, is not as critical for CARMs having a broad amplification bandwidth (see Fig. 7) as it is for a backward wave oscillator (BWO) [18–20] having only one possible frequency of operation.

Metallic structures near to the CARM, like the ion cyclotron resonance antennas in ASDEX upgrade, do not perturb the dispersive characteristics [21]: For a good coupling im-

pedance between the beam and the metallic structure, the beam diameter should be smaller than $\lambda/4$ [17], where λ is the wavelength of the maser radiation. For a beam radius equal to the gyroradius of here 3.6 mm and $\lambda/4=0.6$ mm, this condition is not fulfilled.

The wave moving along the bent path in the tokamak can be approximated by one moving along a straight path, if the phase difference of the wave between the inner and outer radius of the resonant beam, $R_C \pm r_B$ (r_B is the beam radius) is negligible. This is expressed by the relation [22]

$$R_C \gg \left(\frac{L_R^3}{\lambda}\right)^{1/2} \tag{8}$$

($L_R=\pi r_R^2/\lambda$ is the Rayleigh diffraction length). With the gyroradius as beam radius this condition is easily fulfilled: $(L_R^3/\lambda)^{1/2}=3.8$ cm$\ll R_C=2.15$ m. So the maser instability of the runaway electrons can be described by a linear CARM in vacuum.

By numerically solving the cubic dispersion relation of a CARM undergoing the collective instability (see Appendix B) the gain of the maser

$$G=\exp[-\mathrm{Im}(\lambda)\tau] \tag{9}$$

is calculated. $\tau=2\omega_{ce}\rho(\gamma_r^2/\gamma_0^2)t$ is the normalized time (t is the real time) depending via $\rho=\{[\sin(\vartheta_M)\gamma_0^2\omega_{pR0}]/(4\gamma_r^2\omega_{ce})\}^{2/3}$, $\omega_{pR0}=[(n_R e^2)/(\varepsilon_0 m_e)]^{1/2}$ on the density n_R of the runaway electrons ($\omega_{ce}=2\pi\nu_{ce}$). γ_0, γ_r are the relativistic mass factors of the runaway electrons prior to the masing process and resonant with the frequency to the amplified (see above), respectively. $\mathrm{Im}(\lambda)<0$ is the normalized growth rate, which in general, depends on the density, the energy, and the pitch angle of the runaway electrons. The pitch angle ϑ_M used for calculating $\mathrm{Im}(\lambda)$ is determined by the energy balance between the energy gain in the toroidal electric field and the synchrotron radiation losses near a ripple resonance. The effect of the ripple magnetic field as an undulator is negligible here. For the low densities of the runaway electrons, $\overline{n_R} \lesssim 3\times10^{14}$ m^{-3}, corresponding to the observed current carried by the runaway electrons of 10 kA, it is found that the collective instability takes place in the Compton regime and $\mathrm{Im}(\lambda)$ is independent of n_R. The normalized growth rate reaches its maximum value $|\mathrm{Im}(\lambda)_M|=1$ at the resonance energy $\gamma_r m_e c^2$ (Fig. 8). Thus, exactly the frequency which is spontaneously emitted and thus is resonant with the runaways is amplified, confirming the observation. The half width of the gain curve, $2\Delta\gamma\approx0.24$, for $n_R=10^{13}$ m^{-3} is broader than the width of the calculated distribution function of $2\Delta\gamma<0.18$ (see above). Thus, for calculating the growth rate, the approximation of the runaway electrons' momentum distribution by δ functions is justified.

From the condition $GL\gtrsim1$ a lower limit for the density of the runaway electrons,

$$n_R \gtrsim \left(\frac{2\Delta\nu_{1/2}}{\nu}\right)^3 \frac{B^2}{\gamma_r \sin^2(\vartheta_M)} \frac{\varepsilon_0}{4\pi^3 |\mathrm{Im}(\lambda)_M|^3 m_e} \tag{10}$$

is obtained. The calculated density of the runaway electrons $n_R \gtrsim 2\times10^{13}$ m^{-3} is low compared with the line-averaged density $\overline{n_R}=3\times10^{14}$ m^{-3}. So the assumption of a peaked density profile of n_R for this ohmic discharge is confirmed. This analytical estimate of the runaway density in the resonance zone of the CARM is valid for the zero initial spread of the pitch angle. For a more exact determination of the density of the runaway electrons a numerical simulation of the collective instability, taking into account the momentum distribution of the runaway electrons, which affects the growth rate, must be performed.

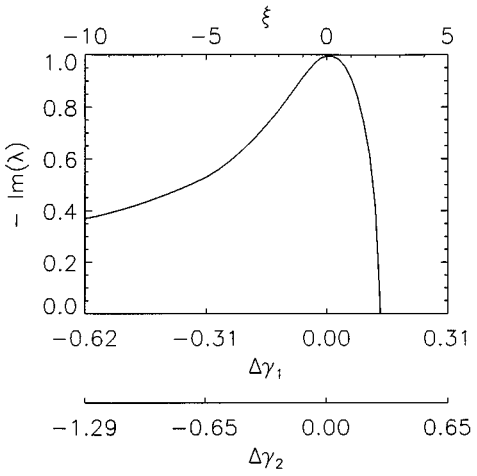

FIG. 8. The normalized gain $-\mathrm{Im}(\lambda)$ (calculated for $\gamma_r=23$, $\vartheta_M=0.207$ rad) does not depend on the density of the runaways in the range $n_R \approx 10^{13}$–10^{14} m^{-3} corresponding to the Compton regime, but on their energy $\gamma m_e c^2$. This is expressed by the normalized quantity ξ and by $\Delta\gamma_i=\gamma-\gamma_r$, with $i=1$ for $n_R=10^{13}$ m^{-3} and $i=2$ for $n_R=10^{14}$ m^{-3}. The maximum growth rate is reached for $\Delta\gamma_i=0$ corresponding to the resonance energy.

To check the value of the runaway electron density, the efficiency of the maser will be estimated in the following. The reflection coefficient R_{PV} at the boundary between plasma and vacuum for an electromagnetic wave resonant with the runaway electrons is $R_{PV}=1/(4\gamma^2)$ [23]. Thus all the energy contained in the amplified wave is observable outside the plasma, allowing the comparison of the measured and theoretical efficiencies of the CARM without any corrections. Since we found the duration of the spikes to be shorter than the time resolution of the analog-to-digital converter of 0.5 ms, we estimate the measured saturation energy with the integrating time constant of the detector system of 1 ms to be $E_S=10$ mW$\times$1 ms, which compared to the energy E_B of the resonant runaway beam (beam length L_P, beam radius equal to the gyroradius of the runways) is $E_S/E_B=3\times10^{-3}$. This is comparable to the theoretical predicted one, $\eta\gtrsim3\times10^{-3}$, calculated from [12]

$$\eta=\left[\frac{\sin(\vartheta_M)\omega_{pR}}{4\omega_{ce}}\right]^{2/3} \tag{11}$$

with $\omega_{pR}=\omega_{pR0}/\sqrt{\gamma_r}$.

IDENTIFICATION OF SIDEBANDS

Due to the limited frequency resolution of 2.6 GHz of each channel, the detection system does not cover the full spectrum of the CARM radiation without leaving holes,

where the emission is unknown. It can, however, be stated that within a frequency difference of 3 GHz the emission intensity decreases from a maximum around 117 ± 1.3 GHz to practically zero at 120 ± 1.3 GHz and increases again to a detectable level at 124 ± 1.3 GHz and 130 ± 1.3 GHz. In the following this upshifted emission of lower amplitude is ascribed to a sideband of the main radiation. Sidebands are generated when the amplification process of the electromagnetic wave saturates and the electrons are being captured in the ponderomotive potential well [12,24]. There they perform synchrotron oscillations with a bounce frequency of (see Appendix C)

$$\nu_b=\nu_{ce}\left(\frac{2}{\pi}\right)^{3/4}\left(\frac{e\gamma_r\tan(\vartheta_M)}{\nu m_e c r_g}\right)^{1/2}\left(\frac{E_S}{\varepsilon_0 L_P}\right)^{1/4} \tag{12}$$

valid for small amplitude oscillations. The sidebands consist then of the lines [25]

$$\nu_S=\nu+N_S\frac{\nu_b}{1-v_{GC}/c}\quad(N_S=\pm1,\pm2,\ldots). \tag{13}$$

The frequency difference between the lines calculated with Eqs. (12) and (13) for the discharge discussed is $\nu_b/(1-v_{GC}/c)=6$ GHz. This explains the shift of the observed first sideband line by 7 ± 2 GHz$\approx$6 GHz and of the second line by 13 ± 2 GHz$\approx2\times6$ GHz. With Eq. (13) one expects to have no radiation intensity at a frequency shift of 3 GHz as confirmed by the nondetectable radiation in the frequency channel sensitive to 120 GHz. At the downshifted side no channel with zero intensity is seen. There could, however, exist one since we do not observe the spectral range between 113.3–115.7 GHz because of restrictions in the detection system. The same is true for the frequency range 106.3–110.7 GHz. The intensity level of the downshifted radiation is similar to the upshifted part. Thus it can be identified as a lower sideband. No further information is available about the fine structure of this spectrum. From the above analysis it is favored that the sidebands consist of single lines instead of a continuum.

There exists a small number of spikes, which appear in frequency channels other than 117 GHz and have no counterpart at 117 GHz. This can be explained by the fluctuating electron density at the plasma edge, which changes the pitch angle of the runaway electrons due to a varying friction force exerted by the plasma on the runaways. The center emission frequency of the runaway electrons then varies with changing pitch angle.

CARM FREQUENCIES AND RUNAWAY ELECTRON PARAMETERS FOR DIFFERENT DISCHARGE PARAMETERS

For different values of the plasma density n_e and the toroidal magnetic field B, the runway electrons achieve different maximum energies $\gamma_r m_e c^2$ (see Table I), as calculated with the Fokker-Planck equation describing their dynamics [2]. The observed fluctuating emission at different frequencies ν_m can be explained by the formation of a CARM as discussed above in detail for discharge No. 4770. The calculated frequencies ν_c coincide with the measured ones ν_m within the errors of measurement and calculation. For determining the density of the runaways from the linewidths $\Delta\nu_{1/2}$ the *observed* values ν_m were used for ν in Eq. (10). This is important for discharge No. 4405, where due to technical restrictions of the detection system, only the second harmonic could be observed. The efficiency η_m for discharge No. 4405, measured from the radiation pulse energy, is much smaller than the theoretical one η, because the main radiation is emitted at the fundamental frequency as confirmed by the other discharges. To increase the accuracy of the results a detection system with an increased frequency resolution must be used.

TABLE I. Comparison of the CARM frequencies and runaway electron parameters for different discharge parameters: $\overline{n_e}$ is the mean thermal electron density of the plasma, B is the toroidal magnetic field at the major radius of 1.65 m. For the runaway electrons the energies $\gamma_r m_e c^2$ resonant with the Nth toroidal ripple resonance and their pitch angle ϑ_M were calculated with a Foker-Planck equation [2]. The observed CARM radiation of frequency ν_m and width $\Delta\nu_{1/2}$ agrees within the errors with the calculated frequency ν_c. The coherence length L_P of the CARM radiation and the density n_R of the runaway electrons was estimated from the linewidth of the CARM radiation. η is the theoretical, and η_m is the measured efficiency of the CARM. In discharge no. 4405 only the second harmonic of the CARM radiation could be observed, which is emitted with a smaller efficiency ($\eta_m\ll\eta$) than the fundamental radiation of the other discharges ($\eta_m\approx\eta$).

	Discharge no.		
	4383	4405	4770
$\overline{n_e}$ (10^{19} m^{-3})	1	1.2	3.0
B (T)	2.14	1.81	2.90
γ_r	33.6	28.6	23.0
N	4	4	8
ϑ_M [rad]	0.162	0.200	0.205
$\nu_m\pm\Delta\nu_{1/2}$ [GHz]	95 ± 3	105 ± 9	116 ± 2
ν_c [GHz]	101 ± 9	132 ± 14	124 ± 8
L_P [m]$\gtrsim$	3.5	2.7	3.2
n_R[10^{13} m^{-3}]$\gtrsim$	6	7	2
η (units of 10^{-3})	5	6	3
η_m (units of 10^{-3})	1.4	0.2	3

CONCLUSION

In a tokamak, a monoenergetic relativistic electron beam, fulfilling the conditions required for a free-electron maser, is inherently prepared and stored. From the emitted frequency the energy of the runaway electrons, and from the observed spectral width and emitted energy per radiation pulse, the particle density of the runaway electrons can be deduced, as was demonstrated. Thus observing this coherent radiation is a different diagnostic for runaway electrons in tokamaks [26]. The energies of the detected extremely monoenergetic runway electrons coincide with the values calculated with the Fokker-Planck equation describing the runaway electrons' dynamics in tokamaks [2], confirming the validity of this model.

ACKNOWLEDGMENTS

We thank W. Suttrop for his support in finding the CARM radiation, as well as U. Schumacher (IPF), H. Röhr, G. Spindler (DLR), and K. Witte (MPQ) for help in understanding this radiation.

APPENDIX A: REFRACTIVE INDEX OF A PLASMA CONTAINING RUNAWAY ELECTRONS

The influence of the electron beam on the refractive index of the medium consisting of a plasma containing high energy electrons has, in the past, been neglected in the analysis of CARMs in plasmas [27–29]. For our application the refractive index of the whole medium is crucial for the guiding of the maser radiation.

The refractive index n is calculated by solving the dispersion relation [formulas (10), (7), and (73) in [11]] of the medium

$$\begin{vmatrix} \epsilon_{11}-n^2\cos(\alpha) & \epsilon_{12} & \epsilon_{13}+n^2\cos(\alpha)\sin(\alpha) \\ \epsilon_{21} & \epsilon_{22}-n^2 & \epsilon_{23} \\ \epsilon_{31}+n^2\cos(\alpha)\sin(\alpha) & \epsilon_{32} & \epsilon_{33}-n^2\sin^2(\alpha) \end{vmatrix} = 0 \tag{A1}$$

(ϵ_{ij} are the elements of the dielectric tensor, where the indices $i,j=1,2,3$ denote the directions perpendicular and parallel to the magnetic field, respectively).

To calculate the dielectric tensor simplifying assumptions are made: The thermal electrons are approximated by cold electrons, because their velocity is much smaller than the speed of light and therefore no kinetic interaction is expected. The distribution function of the runaway electrons being captured in a ripple resonance and having clearly defined parallel ($p_{\parallel 0}$) and perpendicular momenta ($p_{\perp 0}$) is approximated by

$$f(p_\perp,p_\parallel)=\frac{n_R}{2\pi p_{\perp 0}m_e^2c^2}\,\delta\!\left(\frac{p_\perp-p_{\perp 0}}{m_ec}\right)\delta\!\left(\frac{p_\parallel-p_{\parallel 0}}{m_ec}\right) \tag{A2}$$

[n_R is the density of the runaway electrons, the parallel and perpendicular momenta $p_\parallel, p_\perp$ are the arguments of the distribution function f, $\delta()$ is the δ function].

Calculating the elements of the dielectric tensor with formulas (1-2-4) and (10-6-48) in [11] gives

$$\epsilon_{11}=S+\frac{\omega_{pR0}^2}{\omega^2}\left\{\frac{A_0}{D_R}\,\frac{2J_1(z)J_1'(z)\omega}{\gamma_r z}+\frac{B}{D_R^2}\,\frac{J_1^2(z)\omega_{ce0}^2}{\gamma_r n^2\sin^2(\alpha)}\right\}, \tag{A3}$$

$$\epsilon_{12}=-iD-i\frac{\omega_{pR0}^2}{\omega^2}\left\{\frac{A_0\omega}{D_R}\left[\left(J_1'^2(z)+J_1(z)J_1''(z)+\frac{J_1(z)J_1'(z)}{\gamma_r z}\right]+\frac{B}{D_R^2}\,\frac{J_1(z)J_1'(z)\omega_{ce0}\omega\,\sin(\vartheta_M)\sqrt{1-1/\gamma_r^2}}{n\,\sin(\alpha)}\right\}, \tag{A4}$$

$$\epsilon_{13}=\frac{\omega_{pR0}^2}{\omega}\left\{\frac{J_1(z)}{D_R}[2J_1'(z)\cot(\vartheta_M)A_0+J_1(z)\omega\omega_{ce}\cot(\alpha)]+\frac{B}{D_R^2}\,\frac{J_1^2(z)\omega_{ce0}\cos(\vartheta_M)\sqrt{1-1/\gamma_r^2}}{n\sin(\alpha)}\right\}, \tag{A5}$$

$$\epsilon_{22}=S+\omega_{pR0}^2\left\{\frac{2A_0J_1'(z)}{D_R\omega}[J_1''(z)z+2J_1'(z)]+\frac{B}{D_R^2}J_1'^2(z)\times(\gamma-1/\gamma_r)\sin^2(\vartheta_M)\right\}, \tag{A6}$$

$$\epsilon_{23}=-i\frac{\omega_{pR0}^2}{\omega}\left\{\frac{1}{D_R}\left[A_0((J_1'^2(z)+J_1(z)J_1''(z))\gamma_r z\cot(\vartheta_M)+J_1(z)J_1'(z)\cot(\vartheta_M))+J_1(z)J_1'(z)z\,\frac{\omega_{ce0}}{\omega}\cot(\alpha)\right]-\frac{B}{D_R^2}J_1(z)J_1'(z)(\gamma_r-1/\gamma_r)\cos(\vartheta_M)\sin(\vartheta_M)\omega\right\}, \tag{A7}$$

$$\epsilon_{33}=P+\omega_{pR0}^2\left\{\frac{2J_1(z)}{D_R}\left[A_0\,\frac{J_1'(z)n\sin(\alpha)\cot^2(\vartheta_M)}{\omega_{ce0}}+\frac{J_1(z)n\cos(\alpha)\sqrt{1-1/\gamma_r^2}}{\omega}\right]-\frac{B}{D_R^2}J_1^2(z)(\gamma_r-1/\gamma_r)+\frac{[\cot^2(\vartheta_M)-1](2-1/\gamma_r^2)-1}{\gamma_r\omega^2}\right\}, \tag{A8}$$

$$\epsilon_{21}=-\epsilon_{12},\quad \epsilon_{31}=\epsilon_{13},\quad \epsilon_{32}=-\epsilon_{23}. \tag{A9}$$

ω is the radian frequency of the propagating wave, $D_R=\gamma_r\omega A_0-\omega_{ce0}$, $A_0=1-n\cos(\alpha)\cos(\vartheta_M)\sqrt{1-1/\gamma_r^2}$, $B=n^2\cos^2(\alpha)-1$, $S=(R+L)/2$, $D=(R-L)/2$, $R=1-\omega_{pe0}^2/[\omega(\omega-\omega_{ce0})]$, $L=1-\omega_{pe0}^2/[\omega(\omega+\omega_{ce0})]$, $P=1-\omega_{pe0}^2/\omega^2$. $J_1(z)$ is the Bessel function of first order with the argument $z=(\omega/\omega_{ce0})n\sin(\alpha)\sin(\vartheta_M)\sqrt{1-1/\gamma_r^2}$. $J_1'(z)$ and $J_1''(z)$ denote the first and second derivative of $J_1(z)$. ω_{pe0} and ω_{pR0} are the plasma frequencies of the thermal and runaway electrons, respectively, ω_{ce0} is the gyrofrequency of the thermal electrons.

The dielectric tensor is purely real, resulting in no growth or damping of the electromagnetic wave due to kinetic effects. An amplification of a wave is only possible by the reactive instability [11], which is identical to an instability of a free-electron maser (see Appendix B).

The refractive index is then calculated by numerically solving the dispersion relation for real wave vector and frequency for a right circularly polarized (extraordinary) wave, and is valid as long as the cold plasma approximation holds, i.e., that n should not be much bigger than 1.

APPENDIX B: GROWTH RATE OF A CARM IN A COLLISIONLESS PLASMA

The CARM growth rates found in the literature [27–30] that are used to interpret maser radiation of suprathermal electrons in space plasmas are based on the collisionless Vlasov equation. For an electron beam describable by δ functions of the momenta, wave growth due to kinetic effects is suppressed and the reactive instability identical with the concept of bunching of the beam electrons is used [11,31,32]. The formalism of this instability, as derived from the Vlasov equation, is equivalent to the description of the amplifying process by the so-called pendulum equation (Sec. 11.6 in [31]). Here the maximum growth rate occurs at a frequency slightly different from the nominal resonance frequency $\nu=\nu_{ce}/[1-n\beta_r\cos(\vartheta_M)]$. Thus there exists a contradiction if these growth rates are applied to the CARM formed by the runaway electrons in a tokamak, that is, the CARM must amplify the electromagnetic radiation which is spontaneously emitted by the runaway electrons at the nominal resonance frequency. For this, however, a slight energy mismatch between the amplifying and the spontaneously emitting runaway electrons must exist, which is impossible for a δ function distribution of the momenta (see Appendix A). This problem is solved by calculating the growth rate for the collective instability, where the assumption of a constant phase of the amplified wave made in the Vlasov equation formalism is omitted and, thus, the maximum growth rate is obtained at the nominal resonance energy of the runaway electrons. For this, the formalism used to describe the collective instability for undulator based free-electron masers (FEM) [12], is extended to a CARM by including the azimuthal bunching.

In an undulator based FEM the perpendicular oscillatory motion is generated by the undulator magnets. In a CARM this is inherent in the gyromotion due to the axial magnetic field. To extend the formalism of a FEM to a CARM, where azimuthal bunching due to a change in the electron energy occurs, the gyrofrequency is expanded in a Taylor series to first order around the resonant relativistic mass factor γ_r

$$\frac{\omega_{ce0}}{\gamma}=\frac{\omega_{ce0}}{\gamma_r}-\frac{\omega_{ce0}}{\gamma_r^2}(\gamma-\gamma_r) \tag{B1}$$

(γ is an arbitrary relativistic mass factor close to γ_r). With the wave vector k_o of the oscillatory motion defined by $k_o v_{GC}=\omega_{ce0}/\gamma_r$, this can be expressed by

$$\frac{\omega_{ce0}}{\gamma}=k_o v_{GC}-\frac{\omega_{ce0}}{\gamma_r^2}(\gamma-\gamma_r). \tag{B2}$$

In the formalism of the FEM, $k_o v_{GC}$ is the frequency of the oscillatory motion in the magnetic field of the undulator. The azimuthal bunching is described by the term $-\omega_{ce0}(\gamma-\gamma_r)/\gamma_r^2$, to first order. The phase relation between a linearly polarized wave and a plane oscillatory motion is the same as between a circularly polarized wave and the gyromotion. Thus only the term for azimuthal bunching must be included in the FEM equations [12]

$$\begin{aligned}
\frac{d\psi_j}{d\tau}&=\frac{1}{2\rho}\left(1-\frac{1}{\rho^2\Gamma_j^2}\right)+\left(\xi+\frac{1}{2\rho}\right)(1-\rho\Gamma_j\sqrt{2\rho\xi+1})\\
&\quad+\frac{i}{\rho\Gamma_j^2}(Ae^{i\psi_j}-\text{c.c.})-\sigma^2\frac{|A|^2}{2\Gamma_j^2}\\
\frac{d\Gamma_j}{d\tau}&=-\frac{1}{\rho}\left[\left(\frac{A}{\Gamma_j}+i\sigma^2\langle e^{-i\psi_j}\rangle\right)e^{i\psi_j}+\text{c.c.}\right]\\
\frac{dA}{d\tau}&=\left\langle\frac{e^{-i\psi_j}}{\rho\Gamma_j}\right\rangle+iA\xi-i\frac{\sigma^2}{2\rho}\left\langle\frac{1}{\Gamma_j}\right\rangle A
\end{aligned} \tag{B3}$$

[$\psi_j=\theta_j-\dot\theta_0 t,\theta_j$ is the difference between the gyrophase of the jth runaway electron and the phase of the electromagnetic wave, $\dot\theta_0=\omega_{ce0}[1-(\gamma_r/\gamma_0)^2]/\gamma_r$, γ_0 is the relativistic mass factor of the runaway electrons prior to the masing process, t is the real time, $\Gamma_j=\gamma_j/(\rho\gamma_0)$, γ_j is the relativistic mass factor of the jth runaway electrons and $\rho=\{[\sin(\vartheta_M)\gamma_0^2\omega_{pR0}]/(4\gamma_r\omega_{ce0})\}^{2/3}$,

$$A=e\alpha_0\exp(i\dot\theta_0 t)\gamma_0\sin(\vartheta_M)/(4m_e c^2\gamma_r^2 k_o\rho^2),$$

α_0 is the amplitude of the electromagnetic wave, $\xi=(\gamma_0^2-\gamma_r^2)/(2\gamma_r^2\rho)$, $\tau=2\omega_{ce0}\rho\gamma_r t/\gamma_0^2$ is the normalized time,

$$\sigma^2=4\rho^2[1+\gamma_0^2\sin^2(\vartheta_M)]/[\gamma_0^2\sin^2(\vartheta_M)]$$

and $\langle\cdots\rangle$

denotes the average over all the masing runaway electrons numbered by the index j].

The term

$$\left(\xi+\frac{1}{2\rho}\right)(1-\rho\Gamma_j\sqrt{2\rho\xi+1})=\omega_{ce0}\frac{\gamma_r-\gamma_j}{\gamma_r^2} \tag{B4}$$

in the equation for the phase ψ_j describes the azimuthal bunching.

Expanding the normalized variables around their equilibrium values

$$A=0+A$$

$$\psi_j=\psi_{0j}+\theta_j,\quad \psi_{0j}=\frac{2\pi(j-1)}{N_R} \tag{B5}$$

$$\rho\Gamma_j=1+\eta_j,$$

(N_R is the number of runaway electrons taking part in the masing process) and inserting the variables A,ψ_j,η_j in the above CARM equations gives, after linearizing with the new variables $X=A$, $Y=\langle e^{-i\psi_{0j}}\theta_j\rangle$, $Z=\langle e^{-i\psi_{0j}}\eta_j/\rho\rangle$

$$\begin{aligned}
&-\frac{dX}{d\tau}+i\left(\xi-\frac{\sigma^2}{2}\right)X-iY-\rho Z=0\\
&\frac{dY}{d\tau}-i\rho X-Z\left[1+\frac{(2\rho\xi+1)^{3/2}}{2}\right]=0
\end{aligned} \tag{B6}$$

$$\frac{dZ}{d\tau}+X+\frac{\sigma^2}{\rho}Y=0.$$

With the ansatz

$$X=A(0)e^{i\lambda\tau},\quad Y=Y(0)e^{i\lambda\tau},\quad Z=Z(0)e^{i\lambda\tau},\quad \text{(B7)}$$

(λ is an eigenvalue of the three coupled maser equations) one receives, from the above equations, the cubic dispersion relation

$$\left(\lambda-\xi+\frac{\sigma^2}{2}\right)\left[\lambda^2-\frac{\sigma^2}{\rho}\left(1+\frac{(2\rho\xi+1)^{3/2}}{2}\right)\right]+2\rho\lambda+\rho\sigma^2+1+\frac{(2\rho\xi+1)^{3/2}}{2}=0 \quad \text{(B8)}$$

which is solved numerically. The collective instability occurs if there exists a complex λ with an imaginary part $\mathrm{Im}(\lambda)<0$. The resulting gain of the maser scales as $G=\exp[-i\mathrm{Im}(\lambda)\tau]$.

APPENDIX C: BOUNCE FREQUENCY OF THE SYNCHROTRON OSCILLATIONS

When the amplification process of a free-electron maser saturates the amplitude of the electromagnetic wave, the wave is so big that the small amount of energy exchanged with the electrons leaves the wave's phase nearly unchanged. In this case, the CARM can be described by the pendulum equation [12,24,31]

$$\frac{d^2\theta_j}{dR_{GC}^2}=-\left[\frac{2\pi\nu_b}{c\beta_r\cos(\vartheta_M)}\right]^2[\sin(\theta_j)-\sin(\theta_r)], \quad \text{(C1)}$$

where θ_j is the difference between the phase of the jth runaway electron and the electromagnetic wave, θ_r is the same as θ_j but for runaway electrons with the resonant energy, R_{GC} is the space coordinate along the guiding center motion of the runaway electrons, and ν_b the bounce frequency. From the basic equation (B3) (see Appendix B) describing the dynamics of the CARM, the bounce frequency

$$\nu_b=\nu_{ce}\left(\frac{2}{\pi}\right)^{3/4}\left(\frac{e\gamma_r\tan(\vartheta_M)}{\nu m_e c r_g}\right)^{1/2}\left(\frac{E_S}{\varepsilon_0 L_P}\right)^{1/4} \quad \text{(C2)}$$

was calculated. It is assumed here that the electric field of the electromagnetic wave interacting with the electrons is constant and of nonzero value only inside a cylindrical volume of length L_P and of a radius equal to the gyroradius r_g of the runaway electrons. When integrating over the space coordinates the resulting electric energy is equal to the radiation pulse energy E_S.

[1] H. Dreicer, Phys. Rev. **115**, 238 (1959).
[2] B. Kurzan, K. H. Steuer, and G. Fuβmann, Phys. Rev. Lett. **75**, 4626 (1995).
[3] W. Köppendörfer *et al.* (unpublished).
[4] N. A. Salmon and A. Eberhagen (unpublished).
[5] V. V. Parail and O. P. Pogutse, Nucl. Fusion **18**, 303 (1978).
[6] H. Knoepfel and D. A. Spong, Nucl. Fusion **19**, 785 (1979).
[7] O. J. Kwon *et al.*, Nucl. Fusion **28**, 1931 (1988).
[8] L. Laurent and J. M. Rax, Europhys. Lett. **11**, 219 (1990).
[9] R. Q. Twiss, Aust. J. Phys. **11**, 564 (1958).
[10] J. Schneider, Phys. Rev. Lett. **2**, 504 (1959).
[11] T. H. Stix, *Waves in Plasmas* (AIP, New York, 1992).
[12] J. B. Murphy and L. Pellegrini, in *Laser Handbook*, edited by W. B. Colson, C. Pellegrini, and A. Renieri (Elsevier Science, New York, 1990), Vol. 6.
[13] W. Heitler, *The Quantum Theory of Radiation* (Clarendon, London, 1966), p. 241.
[14] V. L. Bratman *et al.*, IEEE Trans. Plasma Sci. **PS-15**, 2 (1987).
[15] L. S. Bogdankevich, H. V. Kuzelev, and A. A. Rukhadze, Usp. Fiz. Nauk **133**, 3 (1981) [Sov. Phys. Usp. **24**, 1 (1981)].
[16] M. Botton and Amiram Ron, Phys. Rev. Lett. **66**, 2468 (1991).
[17] J. Feinstein and K. Felch, IEEE Trans. Electron Devices **ED-34**, 461 (1987).
[18] M. M. Ali *et al.*, Phys. Rev. Lett. **65**, 855 (1990).
[19] V. I. Kurilko, Zh. Tekh. Fiz. **51**, 1415 (1981) [Sov. Phys. Tech. Phys. **26**, 812 (1981)].
[20] K. Minami *et al.*, IEEE Trans. Plasma Sci. **18**, 537 (1990).
[21] W. R. Lou *et al.*, Phys. Rev. Lett. **67**, 2481 (1991).
[22] P. Luchini and H. Motz, Nucl. Instrum. Methods Phys. Res. A **272**, 334 (1988).
[23] M. V. Kuzelev *et al.*, Fiz. Plazmy **13**, 1370 (1987) [Sov. J. Plasma Phys. **13**, 793 (1987)].
[24] T. C. Marshall, *Free-Electron Lasers* (Macmillan, New York, 1985).
[25] J. Masud,T. C. Marshall, S. P. Schlesinger, and F. G. Yee, Phys. Rev. Lett. **58**, 763 (1987).
[26] B. Kurzan, K. H. Steuer, and W. Suttrop, Rev. Sci. Instrum. **68**, 423 (1997).
[27] C. S. Wu and L. C. Lee, Astrophys. J. **230**, 621 (1979).
[28] L. C. Lee and C. S. Wu, Phys. Fluids **23**, 1348 (1980).
[29] N. Omidi, C. S. Wu, and D. A. Gurnett, J. Geophys. Res. **89**, 883 (1984).
[30] R. A. Blanken, T. H. Stix, and A. F. Kuckes, Plasma Phys. **11**, 945 (1969).
[31] D. B. Melrose, *Instabilities in Space and Laboratory Plasmas* (Cambridge University Press, Cambridge, England, 1986).
[32] K. R. Chu and J. L. Hirshfield, Phys. Fluids **21**, 461 (1978).